ORIGINAL RESEARCH Open access

Hyperspectral Imaging for Early Detection of Potato Late Blight under Field Conditions

David Thompson[1*], Sarah Mitchell[1], Rachel Adams[2], James Brown[3], Michael Lee[4]

Abstract

Latent infections in seed potatoes serve as a major initial source of inoculum for *Phytophthora infestans*. Eliminating these sources requires identifying affected plants before any visible symptoms appear. By the time symptoms are noticeable to the naked eye, sporulation has typically already started, potentially allowing secondary infections to spread. Furthermore, manually examining every potato plant is impractical. Although hyperspectral imaging can identify *P. infestans* infections at an early stage, models based solely on spectral data lack generalization because local environmental factors, such as soil moisture levels, strongly influence spectra. A new approach for early *P. infestans* detection involves comparing the spectra of infected plants with those of healthy plants cultivated under matching conditions—specifically within the same row—and producing an image that highlights the differences. A convolutional neural network is subsequently trained on these deviation images, allowing it to successfully identify plant infections from separate fields or from later years, grown under comparable conditions but under different circumstances. This technique was assessed under field conditions during a dry season with very limited potato late blight. During this trial, hyperspectral imaging proved unable to detect the infection.

Keywords Convolutional neural network, Hyperspectral imaging, In-field detection, *Phytophthora infestans*, Potato, Processing pipeline

*Correspondence:
David Thompson
david.thompson@usask.ca
[1] Department of AI for Canola and Flax Seeding Rate Optimization, Faculty of Agriculture, University of Saskatchewan, Saskatoon, Canada
[2] Department of Machine Learning for Snowpack and Soil Freeze-Thaw Cycles, Faculty of Agriculture, University of British Columbia, Vancouver, Canada
[3] Department of Precision Agriculture for Canadian Prairies, Faculty of Agriculture, McGill University, Montreal, Canada
[4] Department of Smart Seeding Robotics, Faculty of Agriculture, University of Guelph, Guelph, Canada

Introduction

Phytophthora infestans poses a serious risk to potato cultivation by inducing late blight. This disease occurs annually as an epidemic and, without management, inflicts extensive damage to leaves and tubers, ultimately causing significant yield reductions. In the Netherlands today, roughly 10-15 fungicide spray treatments are applied each season to manage this pathogen. *P. infestans* is notable for its high genetic variability, with increasing resistance developing against many standard fungicides [1]. Latently infected seed potatoes constitute a key primary inoculum source for *P. infestans*. Research indicates that the transmission rate from infected seed tubers to emerging infected plants ranges from approximately 1.5% to 5%, translating into approximately 2 infected plants per hectare [2, 3]. Prompt detection and elimination of infected plants would delay the onset of an epidemic, thereby giving the crop more time for tuber formation. Hyperspectral imaging (HSI) is a relatively recent detection technology with substantial promise. The interaction between host and pathogen produces distinct spatial and temporal changes in the plant's spectral reflectance [4]. Hyperspectral

This is an open access article distributed under the terms of the Creative Commons Attribution-NonCommercial-ShareAlike 4.0 International License (CC BY-NC-SA 4.0), which permits non-commercial use, distribution, reproduction, and adaptation in any medium or format, provided that appropriate credit is given to the original author(s) and source, a link to the license is provided, and any changes made are indicated. Adapted material must be distributed under the same license.

© 2024 The Author(s). | Published by Agro Intelligence Research Press

imaging merges imaging technology with point spectrometry [5]. While imaging supports structural evaluation, spectrometry analyzes how light at particular wavelengths interacts with plant tissues. Laboratory studies have demonstrated the ability of hyperspectral data to reveal presymptomatic *P. infestans* infections [3, 6, 7].

In Kool *et al.* [3], we developed a presymptomatic detection method for the disease using hyperspectral imaging. This involved training a classifier for pixel-level assignment into four categories: 1) healthy tissue, 2) infected tissue, 3) ring tissue expected to die within the following 24 hours, and 4) healthy tissue from an infected plant. Once noise was minimized, statistical evaluation of the combined percentages of the two healthy classes indicated that, starting on the second day post-inoculation, healthy plants were fully categorized as healthy, while infected plants were not. At that point, the human observer had not yet noticed any infection, confirming that HSI could detect infection before visual symptoms appeared. The current paper reports on continued work, where we optimized the approach using glasshouse-grown plants in 2021 before conducting field validation.

Spectral data alone is inadequate for early identification of *Phytophthora infestans*; proper interpretation of imaging information is also essential. This is demonstrated in the following two cases.

A) One trial carried out in 2021 partially repeated the 2020 study. Potato leaves were spray-inoculated with *P. infestans* and processed through the identical pipeline. Even for the 3 plants that developed symptoms three days after inoculation, the classifier determined that all plant images contained over 99% healthy tissue. This outcome revealed a lack of model generalization.

B) We performed a validation test of the original assumption that *Phytophthora* could be detected using only hyperspectral information across different years and experiments. Two trials were arranged in 2021 to identify early-stage *phytophthora* infection. The imaging setup remained the same — the same camera, lighting, and site — and identical potato cultivars were used. Nevertheless, the experiments were separated by three weeks, causing variations in growth-stage lighting and humidity. Following normalization and removal of non-plant elements, a random forest classifier successfully separated untreated plants from the two trials. This confirmed that spectral information alone is insufficient and that the imaging aspect plays a critical role.

These examples clearly show that spectrometry alone cannot reliably detect *P. infestans*. Detecting plant diseases requires including the imaging dimension and comparing directly with reflectance spectra from healthy plants grown under equivalent conditions. This principle serves as the core basis for our strategy. The present study introduces a processing pipeline that derives image data from spectral measurements by contrasting them with data from healthy plants grown under identical circumstances, meaning plants positioned next to the infected ones. The pipeline is shown in **Figure 1**. This strategy holds strong potential for diseases like *P. infestans*, where primary inoculum sources involve fewer than a handful of plants per hectare. Therefore, the great majority of plants emerge healthy. These healthy individuals then provide essential reference data. A field trial was established in 2022 to image and evaluate 960 plants over four weeks. Glasshouse trials relied mainly on leaf inoculation, whereas the field trial used tuber inoculation. Given anticipated differences in host-pathogen dynamics across these inoculation methods, only the pipeline—not the specific model—was evaluated in the field setting.

© 2024 The Author(s). | Published by Agro Intelligence Research Press

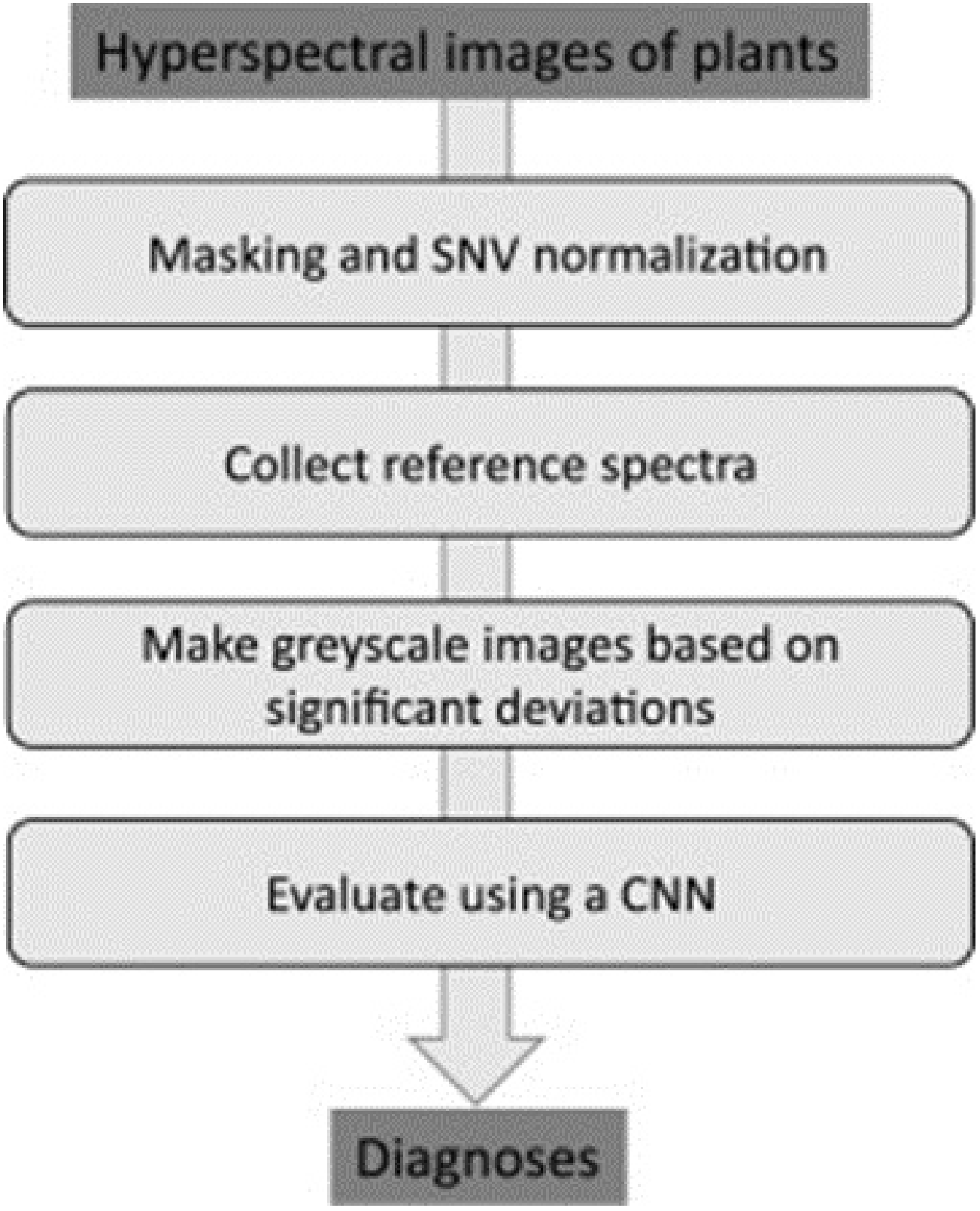

Figure 1. Schematic overview of the data processing pipeline as described in section 2.4.1.

Materials and Methods

© 2024 The Author(s). | Published by Agro Intelligence Research Press

Potatoes and their treatment

Four separate experiments were carried out, all located in Wageningen, the Netherlands.

Experiment A occurred in 2020 and involved 80 potato plants (cv Bintje) assigned to 4 distinct treatments arranged in 20 blocks with a randomized order. The treatments consisted of 1) no inoculation, 2) point inoculation, 3) high-density sporangia spray on leaves, and 4) low-density sporangia spray on leaves. Full details of the inoculation method are available in Kool *et al.* [3]. The dataset for this experiment is accessible at Kool *et al.* [8].

Experiment B was conducted in 2021 and included 45 potato plants (cv Bintje). Of these, 15 were 1) untreated, 2) 15 received spray inoculation, and 3) 15 underwent stem inoculation. Inoculation followed this procedure: A suspension containing 110 EXP5 sporangia per ml of *P. infestans* was obtained by washing sporangia off infected potato slices. Sporangia counts were performed using a haemocytometer, and the concentration was adjusted as required. Droplets of 10 and 100 µl were applied via pipette to potato leaflets, with 4 leaflets inoculated per plant. Plants were placed in a climate chamber at near 100% humidity for 6 hours. Stem inoculation involved applying a 100 µL droplet into the leaf axil; 4 stems were treated per plant, for a total of 60 stems inoculated. Following inoculation, plants were held overnight at 15 °C and high humidity. The underlying data for this experiment are located in Kool *et al.* [9].

Experiment C took place in 2021 with 45 plants (cv Bintje) divided into three treatments, with treatments randomized across 15 blocks. Treatments included 1) no inoculation, 2) tuber inoculation only, and 3) inoculation of both tuber and soil. The procedure was as follows: Around 80 seed tubers were removed from cold storage and preconditioned at 15 °C for one week to promote sprouting. *P. infestans* was first grown on potato slices at 18 °C for one week. A suspension of 110 EXP5 sp /ml was then prepared. Twenty tubers received a 100 µl droplet on an eye and were incubated at 18 °C for another week. On 17 March 2021, healthy tubers were planted in 5-liter pots, for a total of 45 pots. On the same date, an infected seed tuber was placed above 30 healthy seed tubers. Plants grew in a greenhouse. Upon emergence, 15 pots containing both healthy and infected tubers were soil-inoculated with a *P. infestans* suspension on 30 March 2021. Data for this experiment can be found at Kool *et al.* [9].

Experiment D was performed in 2022. Potatoes (cv Agria) were cultivated in a field setting. The design included four replicate blocks, each containing three rows of 80 plants. Row spacing was 75 cm, with plants spaced 33 cm apart. Each row received one of three treatments: 1) no treatment using presumably healthy seed tubers, 2) inoculated seed tubers, or 3) a presumably healthy tuber planted beneath an inoculated seed tuber. Inoculation utilized *P. infestans* genotype EU-36-A2. A suspension of 110 EXP5 sporangia per ml was sprayed onto 720 tubers on 24 May, consuming 2 liters total. Tubers were distributed across 8 trays lined with moist filter paper. Roughly 90 tubers per tray were placed eyeside up. After inoculation, trays were sealed with plastic wrap to maintain high humidity and incubated in the dark at 15 °C for 7 days before planting. Hand planting occurred on 31 May 2022, after which ridges were formed using machinery. The dataset for this experiment is available in Kool *et al.* [10].

Epidemic analysis

A specialist across all four experiments carried out visual inspections for potato late blight. Assessments in experiments A and B happened on days 1, 2, 3, and 6 post-inoculation. Experiment C involved checks immediately after emergence and continued until plants reached around 30 cm in height, on the specific dates of April 6, 9, 16, and 24. Severity ratings in experiments A, B, and C relied on estimates of the proportion of leaf area displaying late blight signs. For experiment D, checks were conducted twice weekly beginning at emergence, noting the presence of *Phytophthora* or *Rhizoctonia*. Late blight evaluations recorded lesions on stems, foliage, or both. Plants that failed to emerge were assigned “X”. Plants suspected of infection received colored markers in the field, with each evaluation date using a distinct color. Molecular testing confirmed true *P. infestans* presence and distinguished whether symptoms stemmed from the applied inoculum or external origins. Conditions in June and July 2022 remained exceptionally dry, leading to minimal late blight development. Data collection began following initial emergence and continued for a full month. Final recordings included removing

© 2024 The Author(s). | Published by Agro Intelligence Research Press

plants from the field for thorough review. Sections with visible symptoms were excised, kept in humid environments, and examined for *P. infestans* sporulation via light microscopy.

In greenhouse trials, foliar blight levels were measured as the proportion of necrotic areas, an indicator of disease intensity. Time-series collections permitted computation of mean severity values. Yet varying gaps between observation points favored the use of the Area Under the Disease Progress Curve (AUDPC). For cross-treatment analysis, AUDPC values were normalized by dividing by the total number of days spanning the initial and final checks, producing the standardized form, StAUDPC.

Stem blight was scored as absent or present. Lesion extent was additionally quantified in cm.

Imaging procedure

Experiments A, B, and C used an Imec Snapscan-VNIR camera inside a darkened enclosure in the glasshouse, spanning 467-900 nm. An Apo-Xenoplan 2.0/20 lens was fitted, with lighting from six 15 Watt halogen bulbs arranged adjacent to the camera. Positioning kept the camera roughly 30 cm overhead, pointed downward. Side-view captures in experiment B targeted untreated and stem-inoculated plants at a similar 30 cm separation. White balance calibration with Spectralon occurred daily at session start and post-shutdown, after allowing the halogen lights to stabilize for 20 minutes. Block arrangements randomized inoculation types within each group. Captures ran daily from approximately 8 am until near 1 pm.

Experiment D employed the Traitseeker platform [11] for image acquisition. This phenotyping system featured a Specim FX10 camera operating across 397-1210 nm, lit by an AEG Halogen lamp (White Xenon H7 55 W 12 V). The platform elevation kept the camera about 30 cm above the highest canopy elements. Its design permitted scanning two rows concurrently. Slower emergence and growth of inoculated tubers increased the effective camera distance beyond 30 cm for those individuals. Colored markers were inserted at infected plant bases during evaluations, facilitating stem tracking through accompanying RGB captures.

Image data analysis

Pipeline

The study sought to build a generalizable model for spotting latently infected seed tubers carrying *phytophthora*, suitable for varied experimental settings and practical field deployment. This led to the creation of a dedicated pipeline depicted in **Figure 1**. Initial operations focus on data masking combined with normalization, accounting for how recorded reflectance levels fluctuate with light-source distance and the plant's volumetric shape. Normalization thus becomes essential. Reference spectrum assembly forms the next phase, recognizing that most field potatoes start healthy and that their reflectance signatures reflect variables such as moisture and nutrient status. Latent infections stand out as irregularities amid the row. Reference spectra from sound plants enable anomaly spotting. The third phase identifies variations and converts them into grey-scale visuals. Isolated spectral shifts are insufficient for solid identification because numerous factors influence them. An examination of the spatial arrangement of these shifts is therefore vital. Phase four applies a convolutional neural network (CNN) to interpret the deviations. For future on-machine field use, the network arrives pre-trained. The ultimate classification labels plants as healthy or affected based on CNN outputs. Further elaboration on each phase appears in the sections below.

Pre-processing

This preprocessing sequence draws on the approach in Asaari *et al.* [12]. Rλ stands for the reflection signal at wavelength λ nm. Each image received a mask generated via an initial normalized difference vegetation index (NDVI) calculation.

© 2024 The Author(s). | Published by Agro Intelligence Research Press

$$\mathrm{NDVI} = \frac{\mathrm{R}_{800} - \mathrm{R}_{670}}{\mathrm{R}_{800} + \mathrm{R}_{670}}. \quad (1)$$

Plant pixels met the criteria of NDVI exceeding 0.55 together with R773 above 0.28. Illumination normalization was then applied to the standard normal variate (SNV) to every pixel x according to:

$$\mathrm{SNV}(x) = \frac{x - \mu(x)}{\sigma(x)}, \quad (2)$$

Where x is the smoothed spectrum vector, μ(x) its average, and σ(x) its deviation. Smoothing of vector x utilized Python's scipy.signal.savgol_filter at window length 7 and polynomial order 3. Subsequent processing operated exclusively on masked SNV data.

Determination of the relevant spectra using experiment A

Experiment A images provided the basis for pinpointing key spectra associated with infection. Extraction on day two post-inoculation covered three tissue types: 1) healthy leaf areas from untreated plants, 2) infected zones, and 3) surrounding ring tissue destined to become necrotic within 24 hours. Averages and deviations were derived for each class. Let (μh(λ), σh(λ)) and (μr(λ), σr(λ)) indicate the means and deviations at λ for healthy and ring tissues. Conditions held that for λ from 745 nm to 765 nm, (μr(λ) + σr(λ)) − (μh(λ) − σh(λ)) remained under 0.27σr(λ), while for λ from 860 nm to 890 nm, (μh(λ) + σh(λ)) − (μr(λ) − σr(λ)) stayed below 0.7σr(λ). These ranges qualified as pertinent. **Figure 2** displays the corresponding means and spectra.

© 2024 The Author(s). | Published by Agro Intelligence Research Press

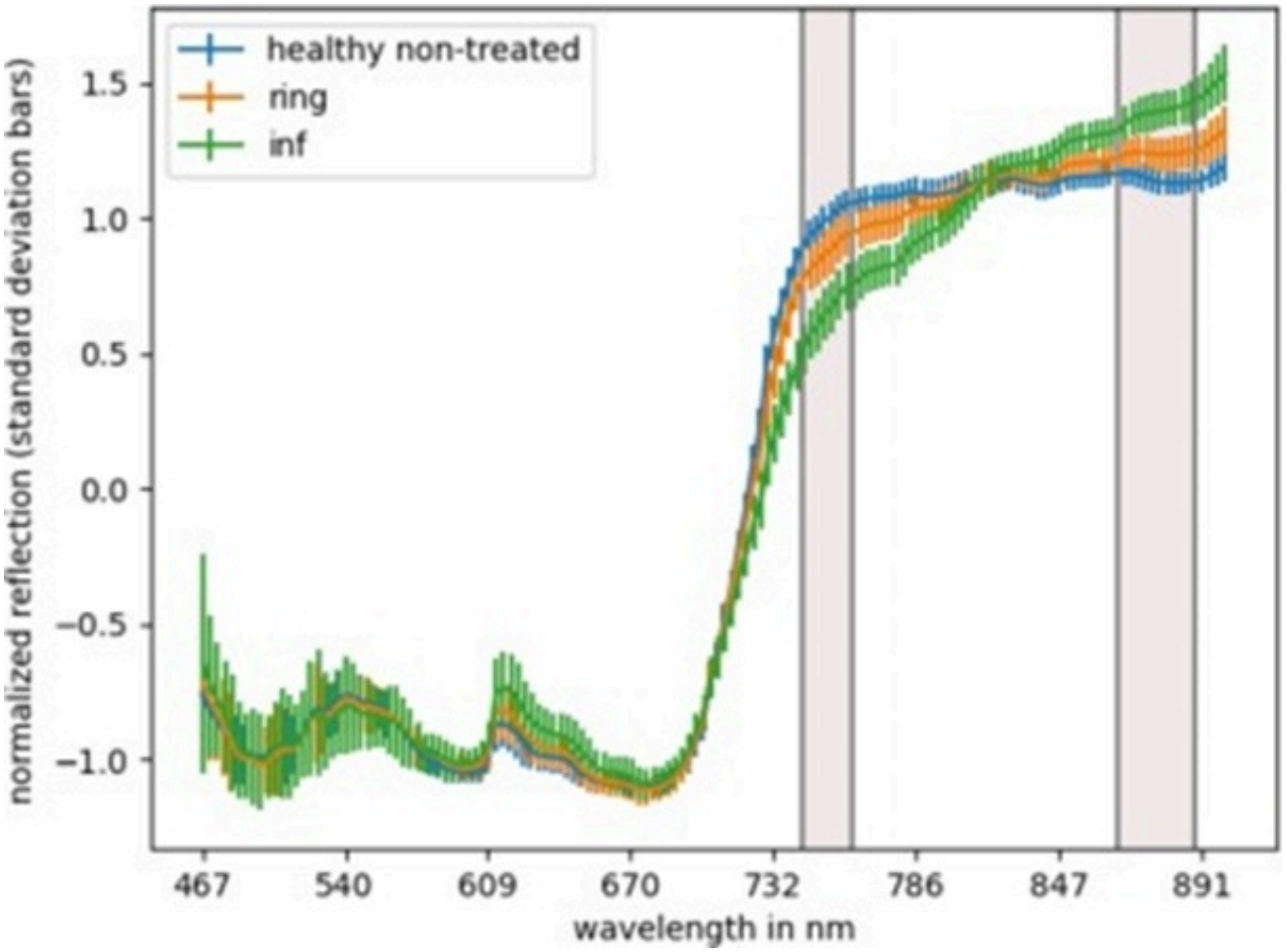

Figure 2. The means for the preprocessed spectra from the images taken from the plants from experiment A, the second day after inoculation. Inf are the spectra of the infected tissue, and ring are the spectra around the infected tissue. The bars show the standard deviations.

Creating the grey-scale images

Grey-scale image generation followed this sequence. Healthy plant spectra were first assembled: non-treated healthy specimens in experiments A, B, and C; non-inoculated rows free of *Rhizoctonia* in experiment D. Per pixel, counts were made of bands from 745 nm to 765 nm dropping beyond 2 standard deviations, plus bands from 860 nm to 890 nm rising beyond 2 standard deviations. Multiplication of the mean decreasing-band count by the mean increasing-band count from those intervals formed the grey-scale result, restricting non-black pixels to those showing concurrent shifts. An illustration appears in **Figure 3**.

© 2024 The Author(s). | Published by Agro Intelligence Research Press

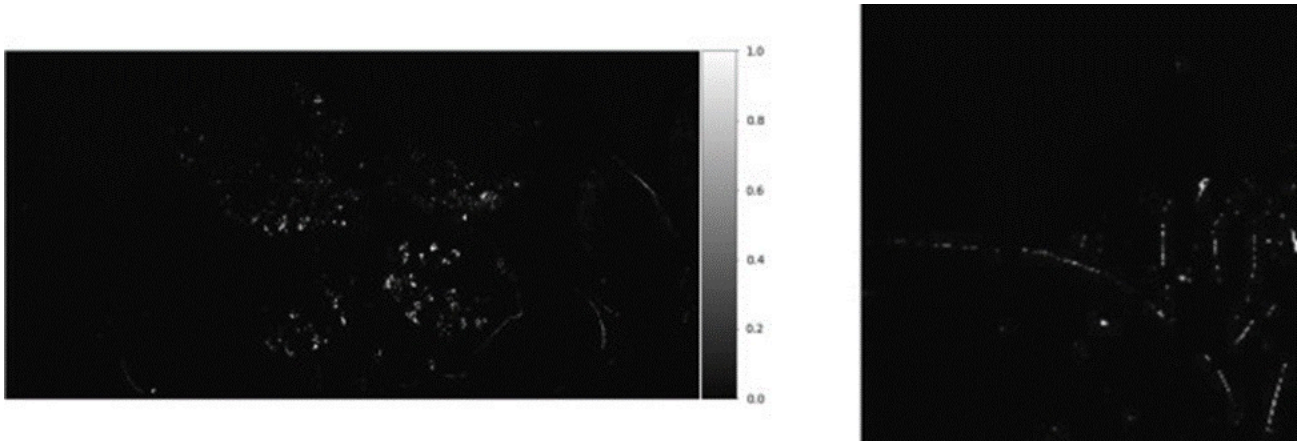

Figure 3. Left) An example of a whole image in which the changes were determined. Parts of these images were used to train a convolutional neural network. Right) An example of such a part, coming from experiment B.

Determination of the relevant spectra for experiment D

Grey-scale outputs generated for experiment D resulted in entirely black visuals. Additional details are available in section 3.3. To assess potential infection visibility, F-statistics were calculated to compare healthy versus infected specimens. This statistic equals the ratio of between-group variance to within-group variance, thereby evaluating differences between groups. Let D signify all samples originating from diseased plant matter, and U signify all samples from UTC matter; further, let $\bar{\lambda}D$, $\bar{\lambda}U$, and $\bar{\lambda}$ represent the average values respectively for D, U, and their union D∪U. For each element x inside a group X, λx corresponds to the value at wavelength λ for spectrum x. Computation of the F-statistic follows:

$$F(\lambda) = \frac{MSB(\lambda)}{MSW(\lambda)} \quad (3)$$

Where:

$$MSB(\lambda) = (\bar{\lambda}_D - \bar{\lambda})^2 + (\bar{\lambda}_U - \bar{\lambda})^2 \quad (4)$$

Indicates the between variance component, and:

$$MSW(\lambda) = \sum_{d \in D} (\lambda_d - \bar{\lambda}_D)^2 + \sum_{u \in U} (\lambda_u - \bar{\lambda}_U)^2$$

(5)

Denotes the within variance component.

Calculations of F-values involved contrasting inoculated plants exhibiting symptoms with non-inoculated, disease-free plants and with inoculated plants lacking symptoms, and the results are plotted in **Figure 4**.

© 2024 The Author(s). | Published by Agro Intelligence Research Press

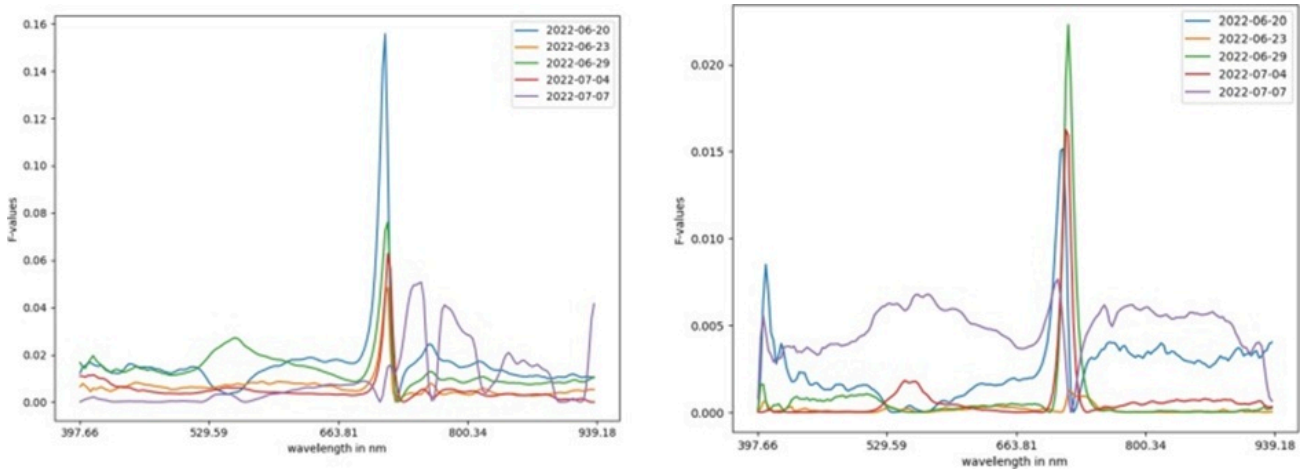

Figure 4. Left) F-values comparing the plants grown from inoculated tubers that showed symptoms with the non-inoculated tubers. Right) F-values comparing the plants grown from inoculated tubers that showed symptoms with the plants grown from inoculated tubers that did not show symptoms.

Creating a CNN for experiments A and B

The plants documented in experiment A were randomly partitioned into training and test groups (14 blocks for training and 6 for testing). Masks in JPEG format were generated from 200 x 200-pixel segments evaluated across a grid spaced at 20-pixel intervals; a segment qualified for inclusion only if its upper-left coordinate (x, y) ensured that at least half its pixels contained plant tissue. An illustration of grey-scale image observation is shown in **Figure 3**. The training JPEGs were further divided into training and validation portions (70% and 30%, respectively). Usage was restricted to JPEGs captured 2 and 3 days following inoculation, producing 1983 items for training, 850 for validation, and 1178 for testing.

Training a convolutional neural network was performed on these images. The network design is depicted in **Figure 5**. The implementation used PyTorch 1.10.0 and binary_cross_entropy as the loss function. Various epoch quantities, learning rate values, and batch size options were tested on the training portion and evaluated on the validation portion. Assessment of effectiveness began with loss examination before proceeding to accuracy evaluation.

```
CNNdeepsigmoid(
  (conv1): Conv2d(1, 20, kernel_size=(3, 3), stride=(2, 2), padding=(1, 1))
  (pool): MaxPool2d(kernel_size=2, stride=2, padding=0, dilation=1, ceil_mode=False)
  (conv2): Conv2d(20, 10, kernel_size=(3, 3), stride=(2, 2), padding=(1, 1))
  (conv3): Conv2d(10, 10, kernel_size=(4, 4), stride=(2, 2), padding=(1, 1))
  (conv4): Conv2d(10, 5, kernel_size=(4, 4), stride=(2, 2), padding=(1, 1))
  (conv5): Conv2d(5, 1, kernel_size=(4, 4), stride=(2, 2), padding=(1, 1))
  (lin): Linear(in_features=9, out_features=2, bias=True)
  (sigmoid): Sigmoid()
```

Figure 5. The architecture of the convolutional neural network.

Initial evaluation of the model took place on test plant images drawn from experiment A. Subsequent plant-scale assessment covered images from both experiments A and B according to two distinct methods:

1. Majority measurement: the dominant outcome among predictions belonging to one plant governs the overall plant classification.

2. Strict measurement: declaration of any individual plant image as diseased triggers classification of the complete plant as diseased.

© 2024 The Author(s). | Published by Agro Intelligence Research Press

Analysis of the stems in experiments B and C

Side-view captures were acquired in experiment B to investigate the detectability of *P. infestans* on stems. These images also received SNV treatment. Application of F-statistics (refer to section 2.4.5) enabled identification of the 10 bands holding the greatest informational value, illustrated in **Figure 6**. Training of a random forest model on those 10 bands utilized Python sklearn configured with n_estimators=75 and max_features='sqrt'. Pixel-wise classification within stem images employed this model, relying on the share of UTC-labeled pixels to separate untreated stems from affected ones. Application of the same model extended to quantifying UTC pixel shares on side-view stem images sourced from experiment C.

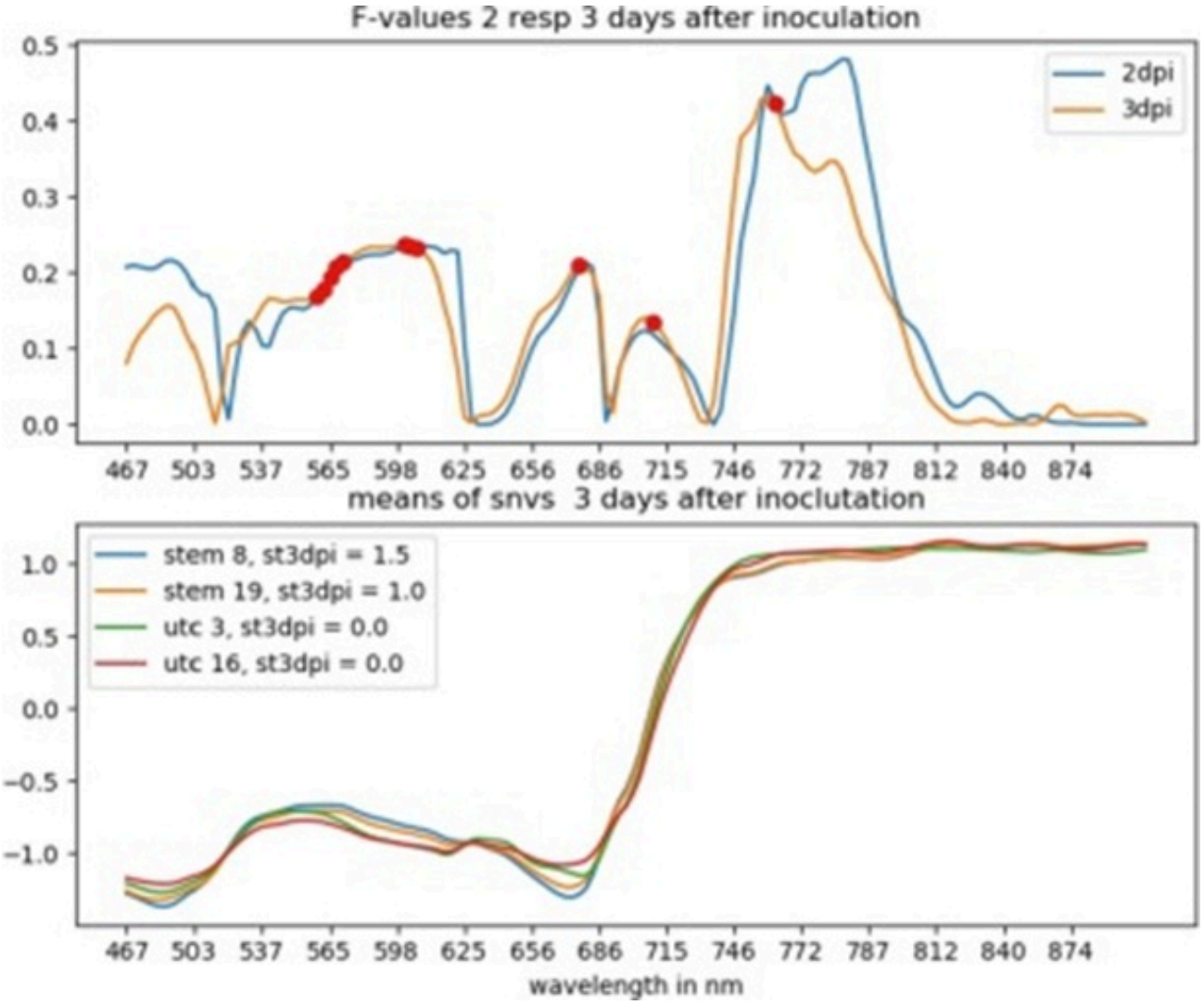

Figure 6. On the top, the F-statistics of the stem signal 2 and 3 days past inoculation. The red dots are the selected bands where the F-statistics are rather high. The bottom graph gives the mean SNV signal of 4 different plants. Two plants were stem-inoculated, and two were not. The st3dpi in the legend indicates the severity of the infection.

Results and Discussion

Epidemic analysis

© 2024 The Author(s). | Published by Agro Intelligence Research Press

Water-treated specimens in experiment A remained free of *P. infestans* signs. Complete symptom development occurred in all inoculated plants, resulting in 100% incidence across the three inoculation variants. Earliest signs emerged two days after point inoculation in the form of small spots detectable only with difficulty by unaided vision. Spray inoculation first yielded visible signs on day three, unaffected by sporangia concentration. StAUDPC-based severity levels varied markedly by treatment. Point inoculation produced substantially higher StAUDPC values than spray methods. High-density spray produced markedly greater StAUDPC outcomes than low-density application.

Experiment B recorded zero symptoms among water-treated plants. Inoculated individuals reached 100% incidence with both leaf and stem applications. Leaf symptoms first manifested three days post-inoculation. Stem symptoms likewise appeared at the three-day mark. Leaf-based inoculation seldom triggered stem involvement, with only 3.6% of stems affected via spread from the leaf petiole. Stem inoculation generated no foliar effects.

No late blight occurred among untreated controls in experiment C. Treatment 2, limited to tuber inoculation, produced infected stems in 5 of 15 plants, yielding a 33% incidence. Treatment 3, combining tuber and soil inoculation, affected 6 of 15 plants, resulting in a 40% incidence.

Treatment influenced emergence rates in experiment D. Full 100% emergence was observed in both the untreated control (treatment 1) and the double-planting setup (treatment 3). Sole use of infected tubers (treatment 2) achieved only 88% emergence, a statistically lower figure. The timing of emergence under treatment 2 also lagged significantly behind the alternatives. Verified late blight signs first appeared on 11 July, amounting to 41 days post-planting. Incidence opened at 3.5% before climbing to 10.8% within three days. Treatment exerted a notable influence on the incidence figures recorded on 11 July. Double-planting registered a 6% incidence, surpassing the untreated control's 0.6%. Infected-tuber incidence was 3.6%, aligning closely with the remaining treatments. Subsequent incidence rises were measured at 16%, 7%, and 6%.

Performance of CNN for experiments A and B

Sigmoid activation in the CNN's terminal layer supplied probability estimates regarding the diseased status of images. Application of a 0.5 probability cutoff for decisions produced accuracies of 78% (training), 80% (validation), and 73% (test) on segmented images from experiment A. Experiment B yielded 44% performance. Classifier ROC curves are shown in **Figure 7**. Plant-wise review for experiment A is summarized in **Table 1**.

Table 1. The performance of the CNN model in experiments A, 2, and 3 days after inoculation.

Category	2dpi–Test plants	2dpi–All plants	3dpi–Test plants	3dpi–All plants
Total number of plants	16	57	16	54
Total diseased plants	10	37	10	35
Total non-diseased plants	6	20	6	19
Classification outcome	**2dpi–Test plants**	**2dpi–All plants**	**3dpi–Test plants**	**3dpi–All plants**
Diseased plants: at least one segment classified as diseased	10 (100%)	36 (97%)	9 (90%)	34 (97%)
Non-diseased plants: none of the segments classified as diseased	2 (33%)	8 (40%)	3 (50%)	8 (42%)
Diseased plants: the majority of segments classified as	6 (67%)	27 (73%)	8 (80%)	29 (83%)

© 2024 The Author(s). | Published by Agro Intelligence Research Press

diseased				
Non-diseased plants: the majority of segments classified as diseased	6 (100%)	20 (100%)	6 (100%)	18 (95%)

Grey-scale images in experiment D

Predominantly black-and-grey-scale images characterized experiment D, including cases with recorded late blight lesions. **Figure 8** demonstrates this outcome when using a half-standard deviation cutoff rather than 2. Markedly reduced F-statistic magnitudes compared with experiments B and C pointed toward complete undetectability of infection.

Selecting the relevant spectra for experiment D

Acquired F-values registered notably low, above all when contrasting diseased specimens against healthy ones derived from inoculated tubers. Moderately elevated statistics were observed between healthy, non-inoculated plants and their diseased, inoculated counterparts. A larger size among healthy plants, positioning them closer to the camera than slower-growing latently infected counterparts, may partly account for this pattern.

The analysis of the stems in experiments B and C

Accuracy levels for the classifier stood at 99% on training material and 74% on test material from experiment B. UTC pixel percentage distributions for experiment B images are presented in **Figure 9**. Equivalent UTC pixel percentages on stems from experiment C feature in **Figure 10**.

Slower development characterized plants arising from inoculated tubers in experiment D **(Figure 11)**, although symptom absence persisted in many instances. Separation of future-diseased plants from healthy ones was not possible.

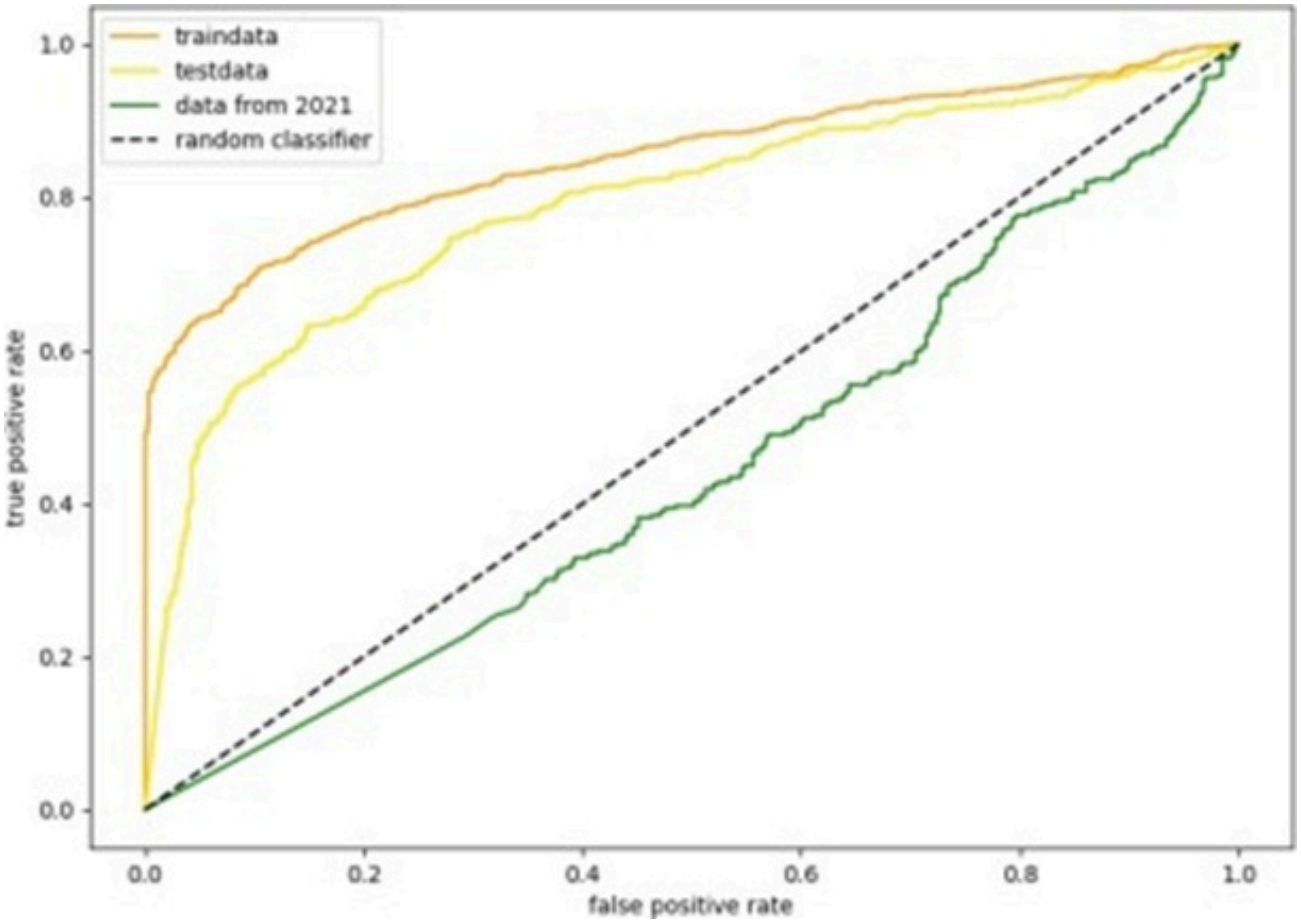

© 2024 The Author(s). | Published by Agro Intelligence Research Press

Figure 7. The ROC curve of the classifier on the training and test data from the 2020 experiment and on the data of 2021.

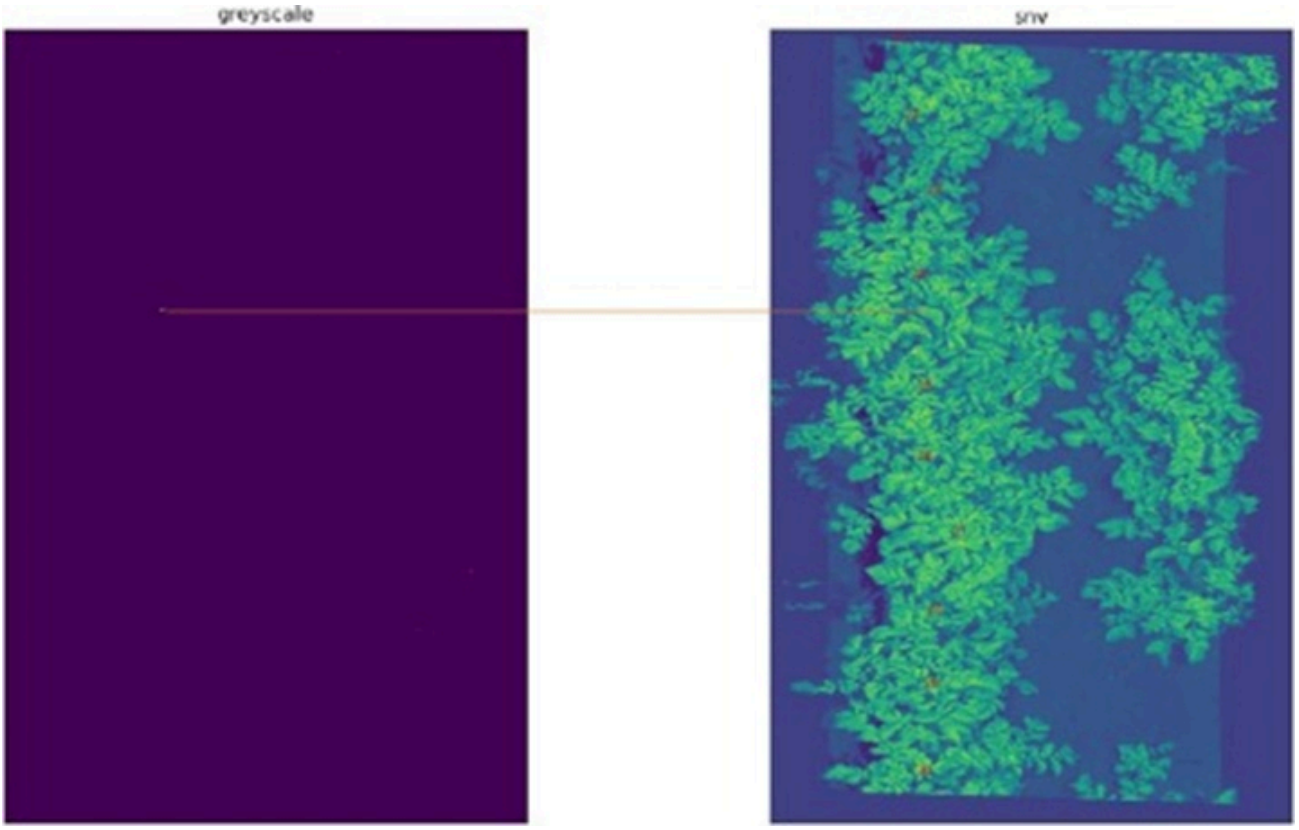

Figure 8. Right) An example of a band from the SNV image, with the plants enumerated in the left row; in plant 24, a lesion was reported. In the grey-scale image left) This is visible. The grey-scale image is generated using half a standard deviation rather than 2. If two deviations had been used, the grey-scale image would have been completely black.

© 2024 The Author(s). | Published by Agro Intelligence Research Press

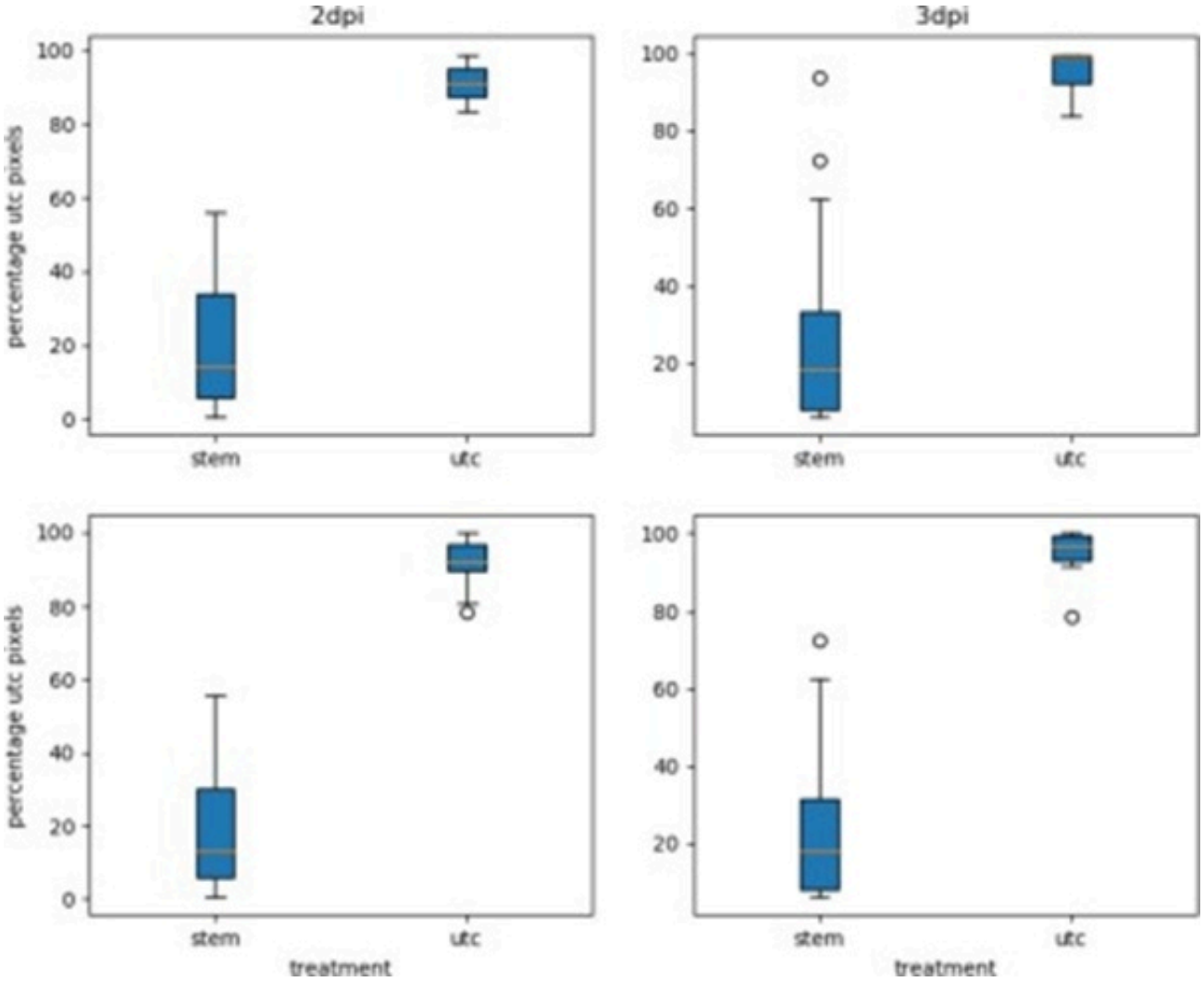

Figure 9. In the top row, the percentages of the UTC-classified pixels of the test plants. For 2 dpi, these were 2 UTC and 23 stem-inoculated plants, and on 3 dpi, these were 5 UTC and 23 stem-inoculated plants. On the bottom row, the percentages of UTC-classified pixels for the plants in the training data set. For 2 dpi, this comprised 9 UTC and 22 stem-inoculated plants, and for 3 dpi, this comprised 9 UTC and 22 stem-inoculated plants.

© 2024 The Author(s). | Published by Agro Intelligence Research Press

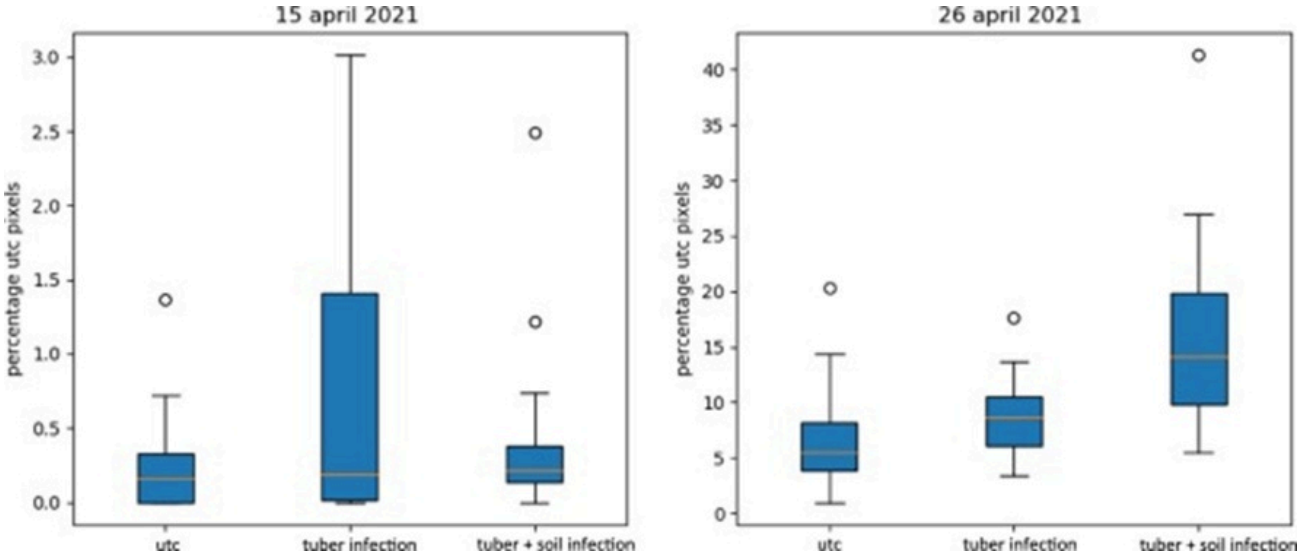

Figure 10. The results of the as utc classified pixels on the stems of experiment C.

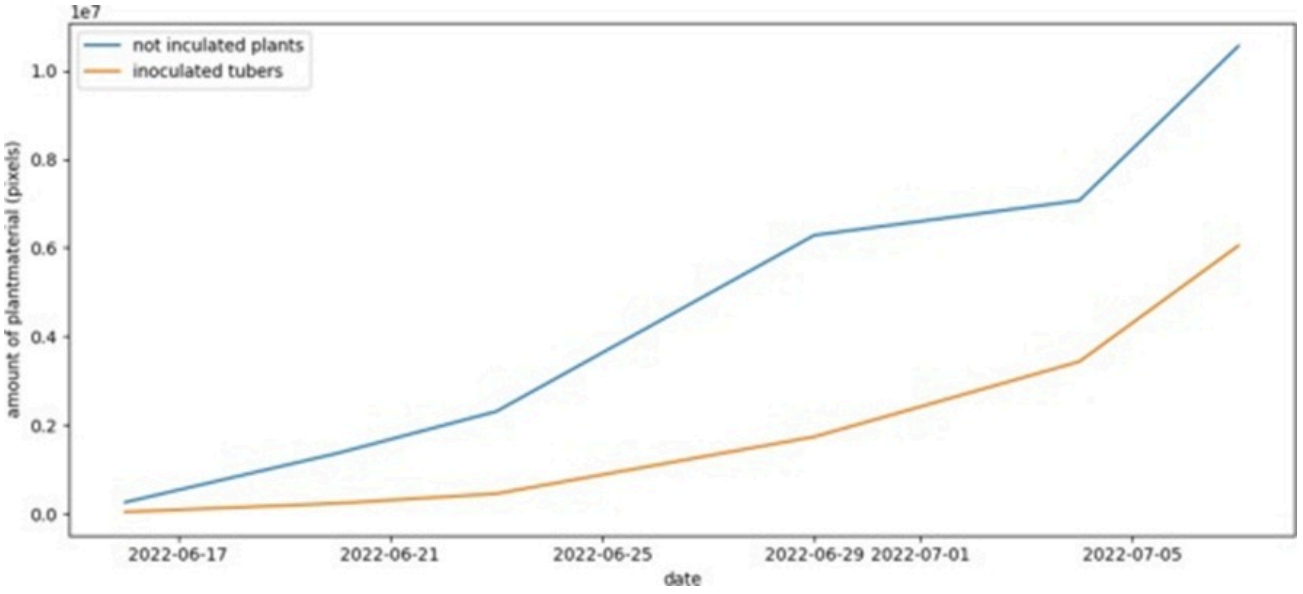

Figure 11. The growth curves of the plants growing from inoculated tubers and non-inoculated tubers in experiment D.

Stem-side imaging in experiment B successfully distinguished inoculated from untreated stems. Replication of this outcome did not occur in experiment C, despite the anticipated pathogen transit from the tuber through stem tissue to the leaves, which would have inflicted stem damage during passage.

Overall, hyperspectral imaging, when paired with the outlined pipeline, does not enable the detection of potato late blight.

Successful artificial inoculation occurred in both experiment A and experiment B, resulting in 100% disease incidence. Symptoms developed rapidly within 2 to 3 days, leaving little time for hyperspectral camera detection before visual identification by a trained observer.

Experiment C replicated a scenario in which latently infected seed tubers were planted under greenhouse conditions. Typically, *P. infestans* infection in a seed potato causes tuber rot and prevents plant emergence, posing no risk to the crop. Alternatively, plants may emerge without subsequent disease development, again presenting no threat. Risk arises

© 2024 The Author(s). | Published by Agro Intelligence Research Press

solely when emergence occurs alongside disease expression. This sequence likely represents an uncommon occurrence in natural settings. To increase the likelihood of observable outcomes, Keil *et al.* [13] implemented a double-planting approach, placing a healthy seed tuber beneath an infested one. The concept stems from the fact that a healthy tuber could acquire infection while passing near the diseased tuber, leading to above-ground infected stems. One variant included additional soil inoculation to promote symptom development further. Tuber inoculation alone produced symptoms on at least one stem in 33% of plants. Soil inoculation raised the incidence slightly to 40%. Infected stems per plant ranged from 1 to 4, while emerged stems per pot ranged from 5 to 14. Untreated controls showed 3 to 7 emerged stems. These figures confirm that both infected and healthy tubers produced stems in the double system. Most infected tubers retained the capacity to generate some stems. Differentiation between stems from healthy versus infected tubers was not achievable.

Limited symptom expression was observed in experiment D despite inoculation of half the planted seed tubers with *P. infestans*. Several plants failed to emerge, likely due to oomycete-induced tuber decay in the soil before stem development. Treatment 2 plants frequently emerged later and remained smaller throughout the trial compared with untreated controls. Nevertheless, the majority of the emerged plants stayed symptom-free during monitoring. Plants that eventually displayed symptoms exhibited lesions on both stems and leaves. Greenhouse trials permitted detection roughly 2 days before the onset of visible symptoms. Comprehensive crop inspection every 2 days is not realistic. Symptom development and secondary spread in the field are influenced by weather patterns, among other factors. Lesions appeared even in untreated controls, albeit at reduced incidence. Such lesions likely resulted from secondary spread from primary infections associated with inoculated tubers within the field. Other nearby sources of infection could also explain their presence.

BlightApp data from Farmmaps [14] identified infection-favorable periods after emergence on 25 and 26 June as well as 1 and 9 July. Initial lesions surfaced on 11 July, two days following the latest favorable period. A 2-day incubation under field conditions qualifies as unusually brief. By 11 July, stem lesions measured several centimeters, while foliar lesions covered approximately half a leaflet and showed active sporulation, as depicted in **Figure 12**. Infections therefore probably occurred during an earlier favorable window, potentially 1 July, according to BlightApp. Note, however, that irrigation in an adjacent field intended to promote late blight may have altered local infection dynamics beyond purely weather-driven effects. No late blight appeared during the 7 July assessment. Lesions might already have existed but remained very small (around 1 mm in diameter) and escaped naked-eye detection. Even the Traitseeker system failed to identify these potential early infections.

© 2024 The Author(s). | Published by Agro Intelligence Research Press



© 2024 The Author(s). | Published by Agro Intelligence Research Press



The initial hypothesis posited that potato plants would exhibit a detectable response to *P. infestans* infection, manifesting as altered reflectance spectra at an appropriate time point. If such a response existed, capture proved unsuccessful. Experiment D particularly demonstrated disease development without producing identifiable spectral shifts. Consequently, the viability of the proposed method for *P. infestans* in potato remains questionable. This outcome does not preclude effectiveness for different crop-pathogen pairings.

Conclusion

Research efforts focused on devising an approach to identify potato late blight at an early stage, before sporulation, using hyperspectral imaging. Reflectance characteristics of plants respond strongly to cultivation environment variables. Spectrum modifications can arise from numerous causes, among them alternative pathogens. Analysis of alteration patterns, therefore, holds importance. Quantification of change patterns drew on observations from experiments A and B. Generalization, however, failed when applying the CNN trained on experiment A material to experiment B records. Divergent symptom manifestation between the tuber and leaf inoculation routes motivated the inclusion of experiments C and D. In experiment D, field conditions produced reflectance shifts too subtle to capture reliably.

Acknowledgements

We want to thank Bert Meurs, Trudy van den Bosch, Florencia Lucca, Corina Topper, and Petra van Bekkum for their help in preparing the material and collecting the data.

This research was made possible with Knowledge Base financing from the Dutch Ministry of Agriculture, Nature and Food Quality, in the project KB-DDHT-38-001-002.

Conflict of interest

None

Financial support

None

© 2024 The Author(s). | Published by Agro Intelligence Research Press

Ethics statement

None

Received: 26 Apr 2023 Revised: 01 Jul 2023 Accepted: 17 Jul 2023
Published online: 25 November 2024

Rights and permissions

Open Access The author(s) retain copyright. This article is licensed under the Creative Commons Attribution-NonCommercial-ShareAlike 4.0 International License. It may be shared and adapted for non-commercial purposes with appropriate attribution, an indication of changes, and distribution of adaptations under the same license. Third-party material may be subject to separate terms identified in its credit line. View the license at https://creativecommons.org/licenses/by-nc-sa/4.0/.

References

1. Schepers HTAM, Kessel GJT, Lucca F, Förch MG, van den Bosch GBM, Topper CG, et al. Reduced efficacy of fluazinam against Phytophthora infestans in the Netherlands. Eur J Plant Pathol. 2018;151(4):947-60.

2. Shattock RC. Winter survival of field isolates of Phytophthora infestans in seed tubers and development of primarily infected plants. Ann Appl Biol. 1976;84(2):273-4.

3. Kool J, Been T, Evenhuis A. Detection of latent potato late blight by hyperspectral imaging. Workshop on Hyperspectral Image and Signal Processing: Evolution in Remote Sensing. 2021. https://doi.org/10.1109/WHISPERS52202.2021.9484002.

4. Mahlein AK, Kuska MT, Behmann J, Polder G, Walter A. Hyperspectral sensors and imaging technologies in phytopathology: State of the art. Annu Rev Phytopathol. 2018;56(1):535-58.

5. Mishra P, Asaari MSM, Herrero-Langreo A, Lohumi S, Diezma B, Scheunders P. Close range hyperspectral imaging of plants: A review. Biosyst Eng. 2017;164:49-67.

6. Fernández CI, Leblon B, Haddadi A, Wang J, Wang K. Potato late blight detection at the leaf and canopy level using hyperspectral data. Can J Remote Sens. 2020;46(4):390-413.

7. Gold KM, Townsend PA, Chlus A, Herrmann I, Couture JJ, Larson ER, et al. Hyperspectral measurements enable pre-symptomatic detection and differentiation of contrasting physiological effects of late blight and early blight in potato. Remote Sens. 2020;12(2).

8. Kool J, Been T, Evenhuis A, Meurs B, Topper C, van Bekkum P. Data underlying detection of latent potato late blight by hyperspectral imaging. Wageningen University and Research. 2021. https://doi.org/10.4121/15081564.

9. Kool J, Evenhuis A, Meurs B, Van Bekkum P. Early detection of Phytophthora in using hyperspectral imaging pot-leaf experiment. Wageningen University and Research. 2021. https://doi.org/10.4121/22203463.

10. Kool J, Evenhuis A, Van den Bosch T, Lucca F. Early detection of Phytophthora in using hyperspectral imaging field experiment. Wageningen University and Research. 2022. https://doi.org/10.4121/22210807.

11. https://www.npec.nl/tool/traitseeker-and-uavs/. 2022.

12. Asaari MSM, Mishra P, Mertens S, Dhondt S, Inzé D, Wuyts N, et al. Close-range hyperspectral image analysis for the early detection of stress responses in individual plants in a high-throughput phenotyping platform. ISPRS J Photogramm Remote Sens. 2018;138:121-38.

13. Keil SB, Benker M, Zellner M. Double setting of potato seed tubers as a new approach to research primary stem blight (Phytophthora infestans (Mont.) de Bary). Am J Potato Res. 2010;87:27-31.

14. https://farmmaps.eu/nl/.

© 2024 The Author(s). | Published by Agro Intelligence Research Press